

4-8-2005

# Teleseismic P-Wave Tomogram of the Yellowstone Plume

H. Y. Yuan

Ken Dueker

University of Wyoming, dueker@uwyo.edu

Follow this and additional works at: [http://repository.uwyo.edu/geology\\_facpub](http://repository.uwyo.edu/geology_facpub)



Part of the [Geology Commons](#)

---

## Publication Information

Yuan, H. Y. and Dueker, Ken (2005). "Teleseismic P-Wave Tomogram of the Yellowstone Plume." *Geophysical Research Letters* 32.7.

This Article is brought to you for free and open access by the Geology and Geophysics at Wyoming Scholars Repository. It has been accepted for inclusion in Geology and Geophysics Faculty Publications by an authorized administrator of Wyoming Scholars Repository. For more information, please contact [scholcom@uwyo.edu](mailto:scholcom@uwyo.edu).

## Teleseismic *P*-wave tomogram of the Yellowstone plume

Huaiyu Yuan and Ken Dueker

Department of Geology and Geophysics, University of Wyoming, Laramie, Wyoming, USA

Received 22 November 2004; revised 25 February 2005; accepted 8 March 2005; published 8 April 2005.

[1] Inversion of a new data set of teleseismic *P*-wave travel-times from three PASSCAL seismic deployments around the Yellowstone hotspot reveals a 100 km diameter upper mantle plume that extends from the Yellowstone volcanic caldera to 500 km depth and dips 20° to the northwest. A monotonic decrease in the velocity perturbation of the plume from -3.2% at 100 km to -0.9% at 450 km is consistent with a uniform thermal anomaly of 180°C. Where the plume crosses the 410 km discontinuity, previous research shows a depression in the 410 km discontinuity consistent with a warm plume (Fee and Dueker, 2004). Additionally, a region of high velocities extends to 250 km beneath the Wind River basin in NW Wyoming that may represent a convective downwelling of the lithosphere. **Citation:** Yuan, H., and K. Dueker (2005), Teleseismic *P*-wave tomogram of the Yellowstone plume, *Geophys. Res. Lett.*, 32, L07304, doi:10.1029/2004GL022056.

### 1. Introduction

[2] From 17–14 Ma, a large-scale magmatic event in the back-arc of the Juan de Fuca subduction zone created the Columbia River basalt group and the eastern Oregon volcanic plateau along with extension and lesser volcanism within the western Snake River Plain and northern Nevada rift [Smith and Braile, 1994; Humphreys *et al.*, 2000]. By 14 Ma, two sets of silicic calderas and domes began propagating outward from SE Oregon: the NE propagating Yellowstone hotspot track (YHT) [Armstrong *et al.*, 1975] and the NW propagating Oregon High Lava Plain trend [Jordan *et al.*, 2004]. Two models for the origin of the YHT remain under consideration. The first model suggests that a modest-sized plume head impacted and spread beneath SE Oregon with a plume tail subsequently migrating to its present location beneath the Yellowstone caldera (YC) [Iyer *et al.*, 1981; Parsons *et al.*, 1994; Smith and Braile, 1994]. A second model suggests that the 17–14 Ma magmatic and extensional events are manifestations of back-arc spreading and that the YHT is not the track of a plume, but instead is a rift along an ancient lithospheric flaw [Christiansen *et al.*, 2002]. Fundamental to testing these differing models is assessment of whether or not a plume tail extends beneath the YC. To date, previous tomographic imaging has lacked sufficient seismic coverage to unequivocally answer this question. This study greatly augments the previous seismic coverage with the addition of data from 76 new Program for Array Studies of the Continental Lithosphere (PASSCAL) stations.

### 2. Data and Methods

[3] Our seismic waveforms are provided primarily by three PASSCAL seismic deployments (Figure 1): the Yellowstone Array (YISA; June 2000 to May 2001), the Billings array (Aug. 1999 to Aug. 2000), and the Snake River Plain array (SRP; May 1993 to Oct. 1993). Events with magnitude  $>5.2 M_b$  and epicentral distance  $>30^\circ$  are selected. A multi-channel cross correlation technique is used to measure 14,327 relative travel-time residuals from *P*, *PP* and *PKP<sub>df</sub>* phases. Given the lack of temporal overlap of the three arrays, a baseline array of nine permanent stations that operated concurrently with all three PASSCAL deployments was constructed from National Seismic Network and University of Utah network stations (Figure 1). For each of our PASSCAL arrays, the mean travel-time residual of the baseline stations with respect to each array's residuals was calculated. These time shifts are consistent between baseline stations (Figure S2<sup>1</sup>) and are consistent with the known upper mantle velocity variations: the largest array (YISA) has the smallest static (0.03 s); the Billings array, which resides over high velocity mantle has a negative static (-0.29 s); the SRP array, which dominantly resides over low velocity mantle, has a positive static (+0.21 s). Timing variations induced by crustal heterogeneity are evaluated using *P*-wave receiver function moho times that were mapped to depth using a 3-D shear wave image derived from Rayleigh wave analysis (D. L. Schutt and K. G. Dueker, in review) and assuming a  $V_p/V_s$  ratio of 1.76 (Figure S2). The peak-to-peak amplitude of the crustal timing corrections is 0.35 s, much smaller than the 2.05 s variation of the data set.

[4] The tomographic model space is  $1600 \times 1600 \times 700$  km in the longitude, latitude and depth directions and is parameterized into  $20 \times 20 \times 25$  km constant slowness blocks. Our choice of a 700 km deep model was guided by analysis of the tradeoff between model depth and variance reduction. This analysis shows that model depths  $>700$  km do not provide significant increases in variance reduction (Figure S3). Our one-dimensional background velocity model is the AK135 model [Kennett *et al.*, 1995] with the upper 200 km set to the average shear wave velocity found beneath the YISA and Billings arrays by D. L. Schutt and K. G. Dueker (in review). To account for sphericity, an earth flattening transformation was used. To assess the effects of 1-D versus 3-D ray tracing on our final model, comparison of ray paths through the most anomalous portions of our model was conducted. This shows that ray path variations are  $<15$  km at 200 km depth and  $<40$  km at 500 km depth; these variations are small with respect to the lateral resolu-

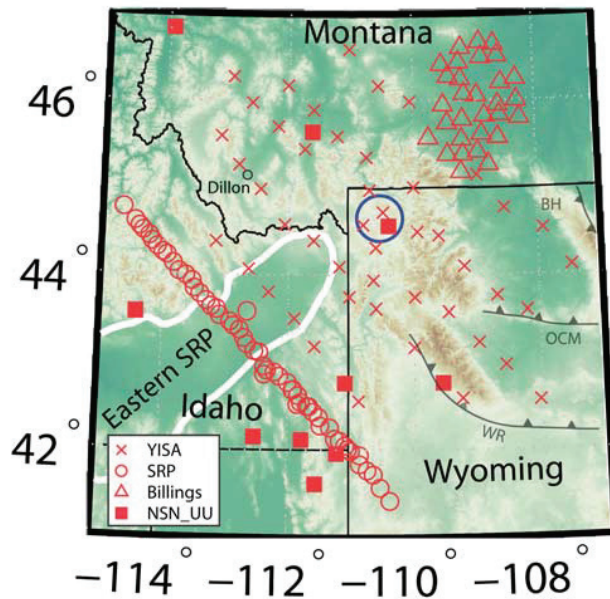


**Figure 1.** Station and topography map. The blue circle is the current location of the Yellowstone caldera. Station associations are shown in legend. The white line outlines the eastern Snake River Plain. Fault labels denote: WR, Wind River; OC, Owl Creek; and BH, Bighorn thrust faults.

tion scalelengths imposed by our regularization. A similar conclusion was found using the SRP array data [Saltzer and Humphreys, 1997].

[5] The matrix equation solved is  $C_d^{1/2} A S S^{-1} m = C_d^{1/2} d$  where  $C_d$  is the a priori data covariance matrix formed from the residual errors,  $A$  is the data kernel matrix,  $S$  is a smoothing matrix with a smoothing half-width of 40 km,  $m$  is the slowness perturbations, and  $d$  is the data residuals. Regularization is imposed using diagonal damping, and the LSQR algorithm is used to invert the matrix problem. Noteworthy is that our use of a 40 km halfwidth data kernel smoothing matrix provides an approximation to the 40–75 km width of a 0.5–2 hz teleseismic *P*-wave Fresnel zone at 150–300 km depths [Hung et al., 2004]. We acknowledge that our use of ray theoretical data kernels will tend to underestimate the magnitude of the velocity anomalies with respect to finite-frequency inversions [Hung et al., 2004]. An important issue in choosing a reasonable damping value is the proper estimation of data errors. The travel-time errors calculated from the multi-channel cross-correlation inversion have a mean standard deviation of 0.06 s. However, this is a lower bound error estimate as it does not contain sources of errors between different events. To quantify this source of error, summary ray values and standard errors were calculated from the polar plot of each station using a summary ray tube width of 0.005 s/km. The mean value of these summary ray errors is 0.09 s and these larger errors are used in our chi-squared calculation. Our best model is slightly overdamped with a reduced Chi-squared value of 12.1 and a data variance reduction of 84%.

### 3. Results and Resolution

[6] Inspection of the *P*-tomography images above 250 km depth (Figure 2) reveals two primary features: a 100 km

wide 2–3% low velocity swath under the east Snake River Plain (ESRP) and Yellowstone Caldera (YC), and a 2–3% curtain of high velocity under the Wind River basin in NW Wyoming. The ESRP anomaly lies directly below the volcanic trough formed by the Yellowstone hotspot track. The NW Wyoming high velocity curtain lies below the region of maximum Laramide thrust fault shortening between the Wind River, Owl Creek and Bighorn faults (Figure 1). Below 250 km depth, this ‘near surface’ velocity pattern disappears and the dominate structure is a low velocity pipe that extends from beneath the YC to ~500 km (Figure 2g). This ~100 km diameter pipe is tilted to the NW at 20° and decreases in amplitude from 3.2% at 100 km to –0.9% at 450 km. This amplitude decrease is consistent with the depth dependence of the anelastic velocity derivatives [Cammarano et al., 2003] and requires a 180° C thermal anomaly. Given these observations, we name this feature the Yellowstone plume. In addition, we note that an ~80 km diameter –0.7% vertical low velocity pipe is imaged in the transition zone about 100 km NW of the YC where the 660 km discontinuity topography indicates warmer than normal mantle (Figures 2f, 2h, and 2i). This low velocity pipe translates into a 120°C thermal anomaly. This pipe is not an artifact due to downward smearing (Figures S4 and S5), albeit upward smearing of structure from below our 700 km model depth is possible.

[7] Two different synthetic data set inversions are presented to illustrate the spatial resolving power and potential artifact creation associated with our tomographic inversion (Figures 3, S4, and S5). The checkerboard spatial resolving power test (Figures 2a–2d) shows that the input structure is reconstructed correctly with >80% and 40% amplitude recovery at 200 and 600 km. The second test consists in the inversion of three synthetic travel-times data sets made from the true velocity model (Figure 2). The three data sets are created by integrating travel-times through the true model, along the raypaths associated with our data set from the surface down to 200, 400 and 700 km depth. To permit comparison with the true velocity image, these data sets had Gaussian noise with a standard deviation of 0.09 s added and the data were inverted to have the same variance reduction as the true model. Inspection of the velocity images for the 200 and 400 km depth synthetic data sets (Figures 3e–3f) show that the base of the Yellowstone plume velocity anomaly is only smeared downwards by ~50 km in each reconstruction. These synthetic tests also provide insight into the level of artifact creation in the transition zone. Inspection of the map and cross sectional views of the 200 and 400 km deep synthetic models (Figures S5–S6) show that little artifact is created below the 200 and 400 km deep synthetic models. To summarize, we conclude that the Yellowstone plume extends to 500 km depth (but no more).

### 4. Discussion

[8] Our most important result is the resolution of a tilted low velocity plume that extends from beneath the YC to 500 km depth. Further support for this conclusion derives from the observation of a localized 12 km depression in the depth of the 410 km discontinuity (Figure 2) where the Yellowstone plume crosses this phase transition (beneath

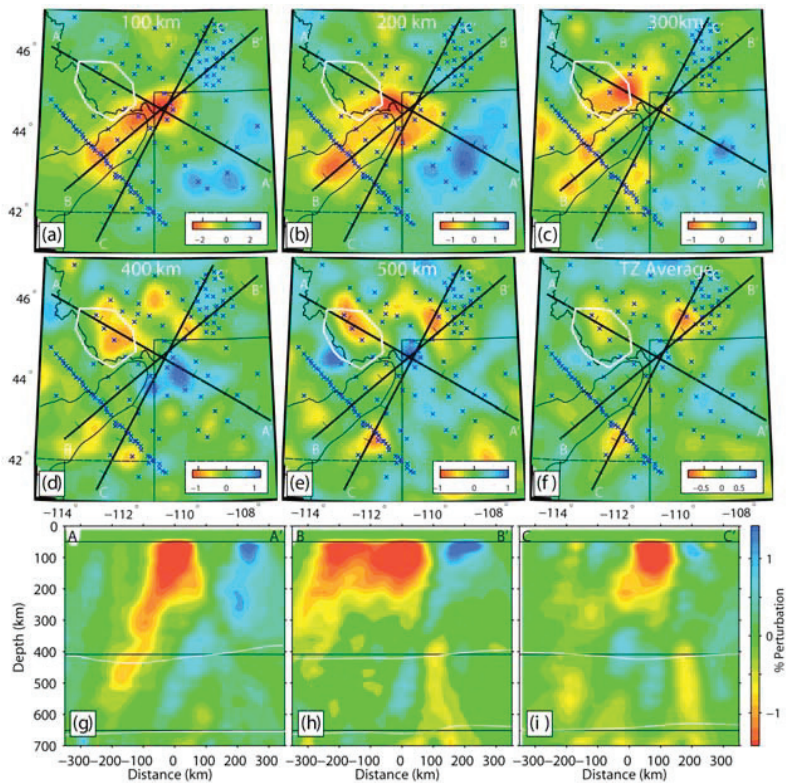


**Figure 2.** Tomographic velocity image. (a)–(f): Map views at indicated depths and the average transition zone velocity structure. Blue crosses are the stations. The white ‘circle’ beneath SW Montana contours the 12 km downwarp of the 410 km discontinuity [Fee and Dueker, 2004]. Cross sections are presented along A–A’, B–B’ and C–C’ in (g)–(i). The x-offset of the cross-sections have a common origin where the three cross-sections intersect at YC. The black lines at 411 and 656 km depth are the mean depths of the 410 and 660 km discontinuities and the white lines are the topography with a factor of two vertical exaggeration. Note that the Yellowstone plume low velocity pipe crosses the 410 km discontinuity where it is downwarped, but the 660 km topography does not show any upwarp associated with a crossing plume.

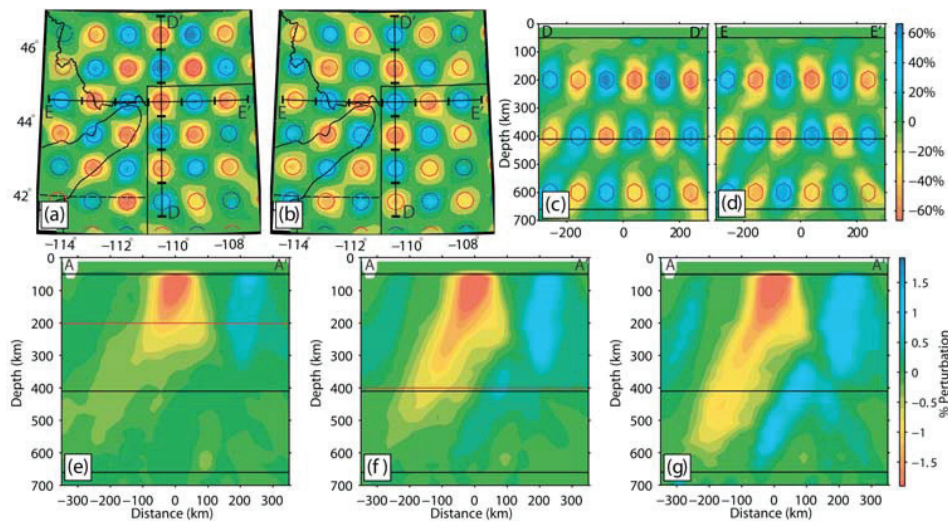


**Figure 3.** Resolution tests. (a)–(d) Checker board test. The red and blue contours outline the 67% amplitude of each input ‘spike’. The spike is a Gaussian function with a 40 km half-width. (a)–(b): Map view at 200 and 400 km depth. (c)–(d): Cross sections along D–D’ and E–E’ shown in (a)–(b). (e)–(g) Images from inversion of three synthetic data sets created by integrating travel-time anomalies through the first 200 km (e), 400 km (f) and 700 km (g) of the true velocity model (Figure 2). The A–A’ cross section is shown in Figure 2. These three cross sections show that the bottom of the Yellowstone plume can be well resolved with <50 km of downward smearing.

Dillon, Montana). Both the 410 topography and the velocity anomaly of the plume are consistent with a 'plume-like' 150–200°C thermal anomaly. The observation of a high velocity anomaly at 400–500 km beneath Yellowstone Park (Figure 2d) is problematic because this anomaly is not observed in the 410 km discontinuity topography. However, Figures S5–S6 suggest that this anomaly may be a velocity artifact created by shallower structure. Regarding a dynamical understanding of the 20° tilt of the plume, calculations of plume conduit advection due to large scale mantle flow show a variety of trajectories for an upper mantle plume [Steinberger, 2000]. While it is noteworthy that most of the Yellowstone plume trajectories tilt to the west, model uncertainties are too large to permit any firm conclusions.

[9] To speculate on the dynamical significance of a plume that stops at 500 km depth, we are guided by two constraints. First, it seems reasonable that a modern-day lower mantle extension of the Yellowstone plume does not exist [Montelli *et al.*, 2004]. Second, two recent global tomographic images resolve a 0.8–1.1% low velocities 'pond' between 700–1000 km depth beneath much of the western U.S. [Grand, 2002; Ritsema and Allen, 2003]. This low velocity pond would be consistent with a ~200° thermal anomaly. Thus, it is possible that the Yellowstone plume originated as a thermal upwelling from this warm pond. A rough estimate of the volume of warm mantle required to make the Yellowstone hotspot track is provided by assuming that the plume impacted the lithosphere around 17 Ma in SE Oregon and that the plume tail has since migrated 700 km to the YC. A proxy for the volume of plume material emplaced below the lithosphere is provided by multiplying the length of the YHT (700 km) by the cross-sectional area of low velocity mantle beneath the ESRP (100 km wide by 100 km deep). Adding this uppermost mantle volume to the volume of the imaged plume conduit (100 km in diameter by 400 km in depth) results in a volume equivalent to a 332 km diameter sphere. Convection modeling shows that the transient release of similar sized warm volumes across the 660 km discontinuity is dynamically plausible [Cserepes and Yuen, 2000].

[10] Finally, we suggest that the curtain of high velocity anomalies extending to 250 km beneath NW Wyoming plausibly represent convective downwelling of the lower lithosphere. These velocity anomalies require 100–150° temperature reduction consistent with lithospheric downwelling models [Schott *et al.*, 2000]. The location of this high velocity curtain adjacent to the Yellowstone plume suggests that this convective downwelling of lithosphere may be balancing the upward flux of plume material. In addition, we note that this region did experience the greatest (15%) Laramide compressive strain [Bird, 1998] between the Wind Rivers, Owl Creek Mountains, and Bighorn thrust faults (Figure 1) which also may have

promoted subsequent convective destabilization of the lithosphere here.

[11] **Acknowledgment.** We thank the PASSCAL instrument center, two anonymous reviewers for their helpful comments and the NSF Continental Dynamics Program that funded this research.

## References

- Armstrong, R. L., W. P. Leeman, and N. E. Malde (1975), Quaternary and Neogene rocks of the Snake River Plain, Idaho, *Am. J. Sci.*, *275*, 225–251.
- Bird, P. (1998), Kinematic history of the Laramide Orogeny in latitudes 24–49 degrees, western United States, *Tectonics*, *17*, 780–801.
- Cammarano, F., S. Goes, P. Vacher, and D. Girardini (2003), Inferring upper-mantle temperatures from seismic velocities, *Earth Planet. Sci. Lett.*, *138*, 197–222.
- Christiansen, R. L., G. R. Foulger, and J. R. Evans (2002), Upper-mantle origin of the Yellowstone hotspot, *Bull. Geol. Soc. Am.*, *114*, 1245–1256.
- Cserepes, L., and D. A. Yuen (2000), On the possibility of a second kind of mantle plume, *Earth Planet. Sci. Lett.*, *183*, 61–71.
- Fee, D., and K. Dueker (2004), Mantle transition zone topography and structure beneath the Yellowstone hotspot, *Geophys. Res. Lett.*, *31*, L18603, doi:10.1029/2004GL020636.
- Grand, S. P. (2002), Mantle shear-wave tomography and the fate of subducted slabs, *Philos. Trans. R. Soc. London, Ser. A*, *360*, 2475–2491.
- Humphreys, E. D., K. G. Dueker, D. L. Schutt, and R. B. Smith (2000), Beneath Yellowstone: Evaluating plume and nonplume models using teleseismic images of the upper mantle, *GSA Today*, *10*, 1–7.
- Hung, S., Y. Shen, and L. Chiao (2004), Imaging seismic velocity structure beneath the Iceland hot spot: A finite frequency approach, *J. Geophys. Res.*, *109*, B08305, doi:10.1029/2003JB002889.
- Iyer, H. M., J. R. Evans, G. Zandt, R. M. Stewart, J. M. Coakley, and J. N. Roloff (1981), A deep low-velocity body under the Yellowstone caldera, Wyoming: Delineation using teleseismic *P*-wave residuals and tectonic interpretations, *Geol. Soc. Am. Bull., Part 2*, *92*, 1471–1646.
- Jordan, B. T., A. L. Grunder, R. A. Duncan, and A. L. Deino (2004), Geochronology of age-progressive volcanism of the Oregon High Lava Plains: Implications for the plume interpretation of Yellowstone, *J. Geophys. Res.*, *109*, B10202, doi:10.1029/2003JB002776.
- Kennett, B. L. N., E. R. Engdahl, and R. Buland (1995), Constraints on seismic velocities in the Earth from travel times, *Geophys. J. Int.*, *122*, 108–125.
- Montelli, R., G. Nolet, F. A. Dahlen, G. Masters, E. R. Engdahl, and S. H. Hung (2004), Finite-frequency tomography reveals a variety of plumes in the mantle, *Science*, *303*, 338–343.
- Parsons, T., G. A. Thompson, and N. H. Sleep (1994), Mantle plume influence on the Neogene uplift and extension of the U.S. western Cordillera?, *Geology*, *22*, 83–86.
- Ritsema, J., and R. M. Allen (2003), The elusive mantle plume, *Earth Planet. Sci. Lett.*, *207*, 1–12.
- Saltzer, R. L., and E. D. Humphreys (1997), Upper mantle *P* wave velocity structure of the eastern Snake River plain and its relationship to geodynamic models of the region, *J. Geophys. Res.*, *102*, 11,829–11,841.
- Schott, B., A. Yuen David, and H. Schmeling (2000), The diversity of tectonics from fluid-dynamical modeling of the lithosphere-mantle system, *Tectonophysics*, *322*, 35–51.
- Smith, R. B., and L. W. Braile (1994), The Yellowstone hotspot, *J. Volcanol. Geotherm. Res.*, *61*, 121–187.
- Steinberger, B. (2000), Plumes in a convecting mantle: Models and observations for individual hotspots, *J. Geophys. Res.*, *105*, 11,127–11,152.

K. Dueker and H. Yuan, Department of Geology and Geophysics, Dept. 3006, 1000 University Ave. University of Wyoming, Laramie, WY 80271–3006, USA. (yuan@uwyo.edu)